Chapter 6

Lithium Irradiated poly(vinylidene fluoride) Nanohybrid Membrane for Radionuclide Waste Management and Tracing

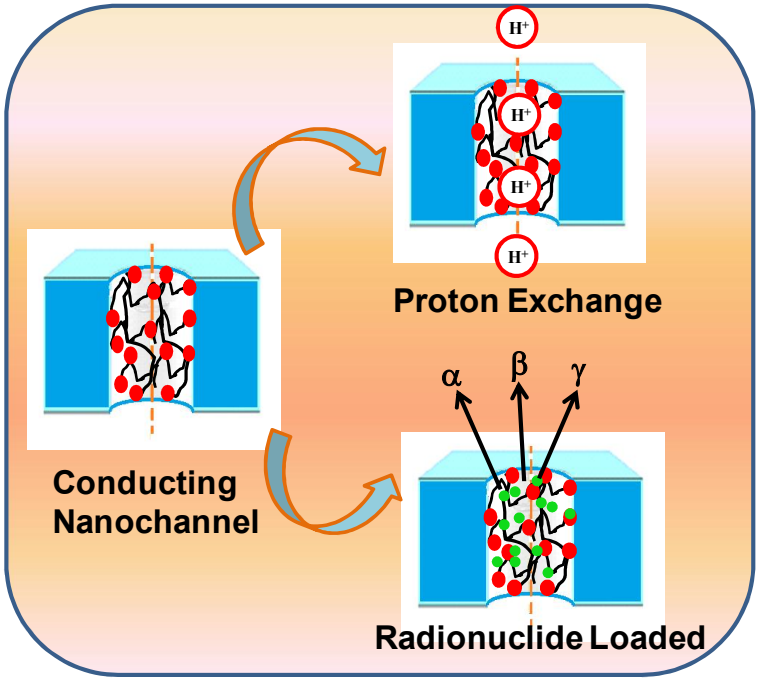

6.1 Introduction:

Membrane technology has continuously been developed into a prominent separation technology over the past few decades. There are many advantages of the membranes especially for the separation process which include light weight, tailor made design, less energy consumptions, low cost, unchanged phase during its use and its easy handling, therefore, they find applications in various fields.[198] One of the most important applications is the radioactive waste management which is generated during the operation of the nuclear facilities worldwide for nuclear energy production using various radioisotopes. Radioactive waste from nuclear fuel cycle in the reactor is a major concern globally as it cannot be disposed off directly into the environment.[25], [110] So, the radioactive waste management is of prime importance [222] along with the detection of the radioactive element using scintillation detector.[223] Radionuclides can be identified/quantified by measuring the various types of primary radiations emanating from the sources, for example, α, β, γ-rays and neutrons or subsequent effects arising from their interaction with matter.[25] Nuclear waste must be stored and processed to a reduced volume for their long term storage for final disposal. This requires separation of long-lived radionuclides, particularly alpha emitters, from the bulk of the nuclear waste, thereby, significantly compressing the volume of the nuclear waste for disposal. The membrane technology plays an important role for removing the different radionuclides such as Am^{+3}, U^{+4}, Pu^{+4}, Np^{+3} and fission products like $^{37}Cs^{+}$, $^{24}Na^{+}$, Ba^{+2} etc.[124] The membrane should have specific functional group so that they form either complex with the radioactive species, mainly in anionic form, or electron rich species from aqueous solutions.[210],[8] Grafted thin film used for the ultrafiltration of the plutonium ions from their large volume

nuclear waste, succeeding to the quantification of the Pu^{+} (pre-concentrated) with the help of alpha-spectrometry [25]. Recording of the energetic charge particles on the polymer film such Solid state nuclear track detectors (SSNTDs) is most accurate, sensitive, easy handing Detector. [223] Different methods are used to incorporate the reactive site in the polymeric membranes to introduce the ionic group in the polymer backbone, such as chemical treatments, UV-visible irradiation, γ-irradiation, metal carbonyl polymerization and bombardment by electrons and high energy ion beams. Amongst these, the bombardment of high energy ion beam such as swift heavy ion (SHI) is the important tool for the reactive species generation in polymeric membranes. [131] During high energy SHI bombardment on substrate, the energy loss occurs through nuclear and electronic collision and chemical as well as physical changes in the polymer do occur due to electronic collision. The changes include the formation of free radical, double bond, chain scissions, byproduct gas evolutions and cross-linking etc.[224] The generated active sites are utilized for grafting of another polymer followed by functionalization to create ionic species like sulphate, phosphate, chlorate, nitrate etc. These membranes have the potential to form complex or ion exchange capability for radioactive waste management.

Fluoropolymer such as PVDF [poly(vinylidene fluoride)] and copolymers of that exhibit unique characteristics such as good thermal and excellent mechanical stability because of their nonreactive and insulating behavior together with their durability Which implies that for membrane material for the radio nuclear waste management . [20] PVDF [poly (vinylidene fluoride)] and that's copolymers subsist five non-identical crystalline phases, some of these are polar/ partial polar and some are non-polar. Polar crystalline phases like β, γ, δ and ε while non-polar phase is α. Among these phases the polar phases exhibits the

piezo/pyroelectric properties in polymer. The electro-active phases / piezoelectric can be introduced in non-polar (α) phase by the addition of some specific fillers [197] Nanofiller polymer composites have fascinating properties in terms of thermal, mechanical performance, ecofriendly nature, and their applications in electronic devices, sensors, defense, automotive, aerospace etc. The homogeneous dispersion of the nanofiller leads to the good interactions with the polymer matrix and exfoliation/intercalation is the key factors for the enhancing their properties. [79] [94] the thermodynamics of mixing of nanofiller and polymer can be described through the balance enthalpic and entropic factors, which determine the nature of nanofiller dispersion in the polymer matrix. [81] Nanofiller dispersion arises from the favorable thermodynamics of mixing and strong interactions suppress the melting temperature and heat fusion in polymer nanocomposites. The surface area of the nanofiller is considered as high enough which impose the entropic increment. [79]

In current work, conducting nanochannels are fabricated by swift heavy ion beam from accelerator, followed by their selective chemical etching and subsequent grafting of nanochannels using styrene monomer to graft polystyrene. Functionalization of the nanochannels are done through sulphonation of the styrene moieties inside the nanochannel to develop the membrane.[8][114][60][197] The functionalized membranes are utilized for radionuclide capture from the aqueous radio-nuclear waste and greater efficiency mechanism understood from their confinement of conducting nanochannels ,Further, functionalized membranes are characterized using electrochemical analyses such as proton conductivity and activation energy calculation. The radionuclide sensing application by the membrane is also demonstrated.

6.2 Experimental

6.2.1Materials:

SOLEF @ 6008, Poly(vinylidene fluoride) (PDI ~2.1) commercial product without any additive with molecular weight 1.45×10^5 $gmole^{-1}$, 30B nanofiller with density 1.98 g/cc was procured from Southern Clay Inc., USA, $KMnO_4$ (potassium permanganate) (LOBA Chemie) AR/ACS grade with purity 99% , sodium Hydroxide (NaOH) purchased from Hi-media, potassium disulfite ($K_2S_2O_5$) purchased from LOBA Chemie with purity 98%, toluene (Himedia) with purity 99.5%, chlorosulphonic acid (HSO_3Cl, LOBA Chemie) with 97% purity, HNO_3 (LOBA Chemie) with 69% purity, HCl (Merck) with 37% purity, styrene monomer (Sigma-Aldrich) regent plus grade with 99.9% pure was vacuum distilled before use.

6.2.2 Functionalization of the membrane:

PVDF and nanoclay dispersed nanohybrid (NH) membranes were thickness around 80 μm irradiated using the Li^+ ions beam with energy 80 MeV in a GPSC chamber (~1×10^{-6} mbar pressure) in IUAC New Delhi India. The ion beam fluences were used 1×10^6 and 1×10^7 ions/cm^2 to ensure sufficient latent tracks produced in the membrane. The irradiation scattering experiment was carried out on thin gold foil (~250 μg/cm^2).The angle between detector and gold foil set 15^0 before the irradiation experiments. After that irradiated membrane chemically etched using the highly alkaline potassium permanganate (9 molar NaOH with 0.25 molar $KMnO_4$) solution at 65 ^oC for 4h. The etched thin films were speedily deep in a potassium metabisulphite ($K_2S_2O_5$) for 30 min go after by washing in double distilled water for removing the brownish precipitate of MnO_2 which is formed during the chemical etchant reactions. The subsidiary water on the surface of chemically

etched membrane was take out with a tissue paper and dried at 65 ^{o}C for 48 h in a vacuum oven under reduced pressure to avoid the oxidation of the reactive sites which is formed during the removal of amorphous zone. The 2×2 cm^2 size etched films were deep in the monomer solution (2 ml distilled styrene monomer in 8 ml distilled toluene) to initiate the grafting process under nitrogen atmosphere. Solution containing the film was stirred (polymerization solution) at 60 ^{o}C for 24 h under nitrogen atmosphere and the unreacted styrene along with homopolymer (pure polystyrene) were washed in toluene for 12 h at room temperature. In the End of the etched films were cleaned with aqueous methanol solution and were dried at 60 ^{o}C for 24 h in vacuum oven. Electrophilic substitution reaction was carried out on the grafted polystyrene using chlorosulphonic acid (HSO_3Cl) at 65 ^{o}C for 30 min. The films were cleaned with double distilled water after the Electrophilic substitution reaction (sulphonation) and were dried at 65 ^{o}C for 24 h in air oven followed by vacuum oven. Mechanically stable polymer functionalized films were obtained after chemical modification for ready use in present application by altering the sulphonation temperature and time. The term PVDF-e, NH-e, refer to the etched PVDF and NH films, respectively. PVDF-6, PVDF-7, NH-6 and NH-7 refer to the grafted and sulphonated respective membranes, while the term '6' refers to the exposure with 1×10^6 ions/cm^2 and the term '7' refers to 1×10^7 ions/cm^2 fluence irradiated specimen. Whole process for the preparation of functionalized membranes is shown in **Scheme 6.1**. The details of the chemical reactions are given in the **Scheme 6.2.**

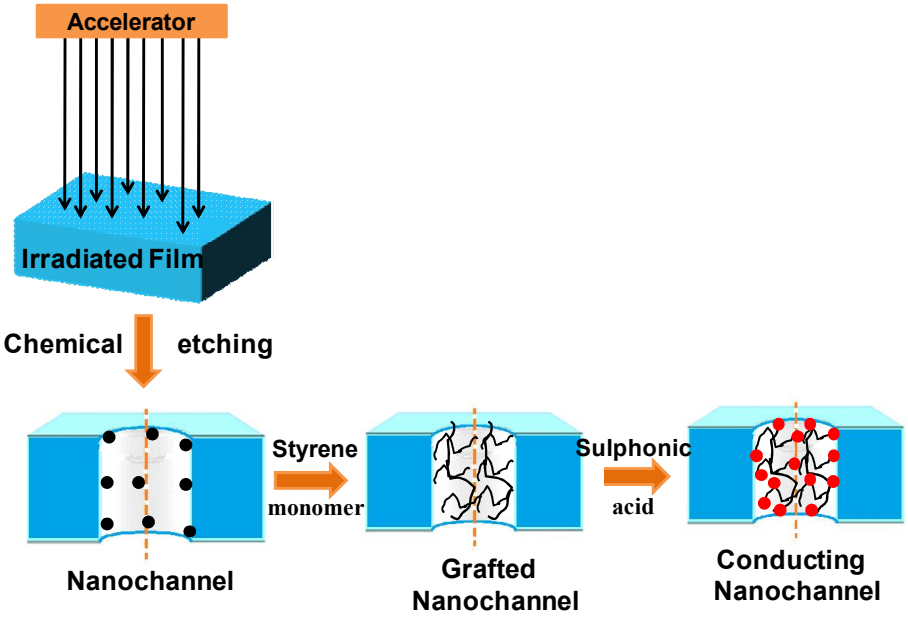

Scheme 6.1: Schematic presentation of the irradiation, nanochannel formation, grafting followed by the sulphonation to generate a functionalized membrane.

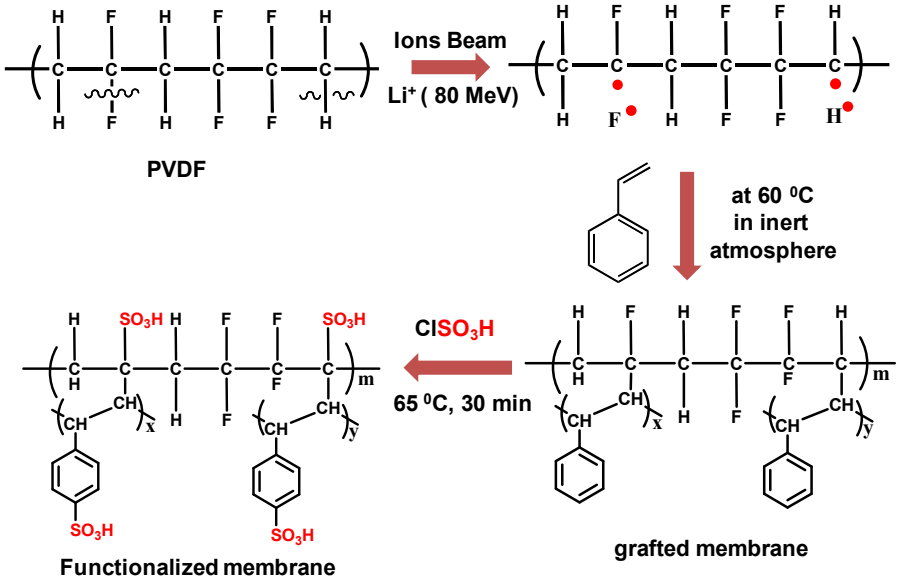

Scheme 6.2*:* Schematic representation chemical reactions of the ion beam bombardment (Li^+ beam) which generate reactive sites (free radicals) followed by grafting using styrene monomer and subsequently the sulphonation using chlorosulphonic acid. This

functionalization converts the nano-dimensional channels into conducting for the ions transport and radionuclide capturing experiments.

6.3 Results and discussion:

6.3.1 Fabrication of nanochannels using SHI:

Interaction of high energy ion beams with the polymer matrices creates latent tracks during its passage through the polymer matrix. While passing through the polymeric thin film, high energy Li^{+} ions (80 MeV) deposits its energy via two processes namely Coulomb stopping and nuclear stopping arising from ion-electron and ion-atom interactions, respectively. Due to the energy transfer of the incoming ions, bond breakage takes place primary to the generation of radicals, predominantly in the latent tracks, along with the bond reorganization within the polymer chains. [8], [48] The passage of swift heavy ions through polymer film produces latent tracks, mostly amorphous in nature, which can be detached easily by chemical etching to create the nanochannels in the polymer film as shown in AFM morphology in **Figure 6.1a**, as indicated by the arrows. There is clear distribution of channel size and the nanochannel dimension increases to 50±5 nm in PVDF-e at 1×10^{7} ions / cm^{2} fluence from the value of 40±5 nm at 1×10^{6} ions / cm^{2} fluence while the size in nanohybrid (NH-e) remain low at ~40 nm (**Figure 6.1b**). Similar results are also found in SEM morphology investigation as shown in **Figure 6.1c** and similar deliberation of the channel dimension through the SEM images was shown in the literature. [8][49] The distribution of channel dimension indicates the inner diameter of 50±5 and 48±5 nm, in PVDF-e under 1×10^{7} and 1×10^{6} fluence, respectively, while 32±5 and 30±5 nm are observed in NH-e at 1×10^{7} and 1×10^{6} fluence (ions/cm^{2}) (**Figure 6.1d**).

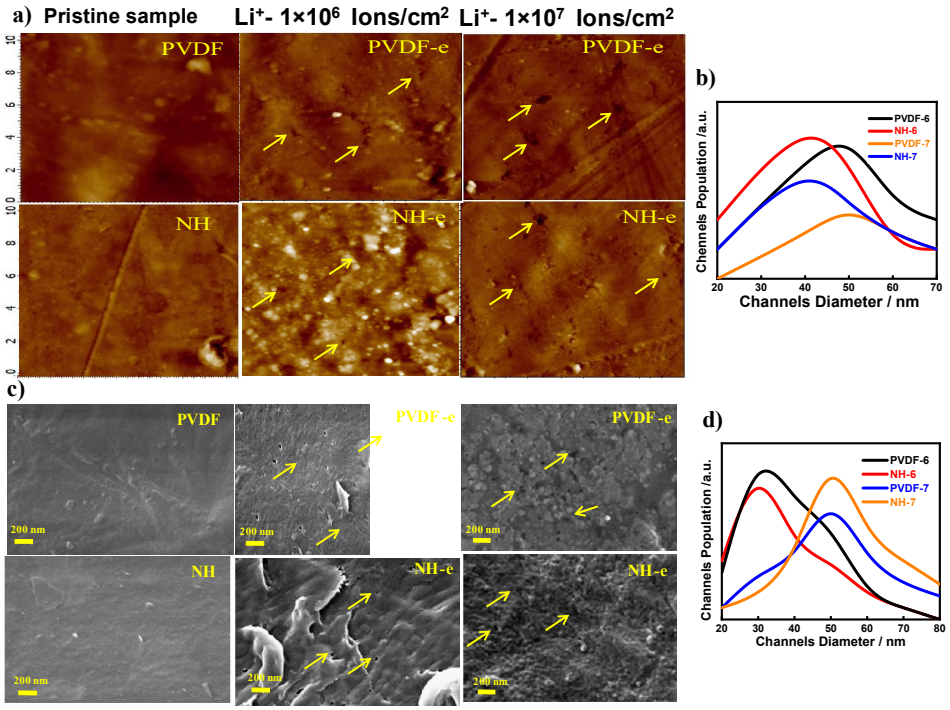

Figure 6.1: Through nanochannel dimension are measured using SEM and AFM morphological investigations, **(a)** AFM images of pristine PVDF, NH, PVDF-e and NH-e showing the nanochannels by arrows under indicated fluence of Li+ ions bombardment; **(b)** the distribution of the nanochannel dimension as measured from the respective AFM images; **(c)** SEM images of pristine PVDF, NH, PVDF-e, and NH-e after the bombardment of Li^{+} ions at indicated fluence and the arrows show the location of the nanochannels; and **(d)** the distribution of nanochannel diameter after the irradiation followed by the chemical etching obtained from SEM images.

3-D images of the porous membrane are presented **Figure 6.2 (a-d)** which indicates the obvious through nanochannel across the depth scale.

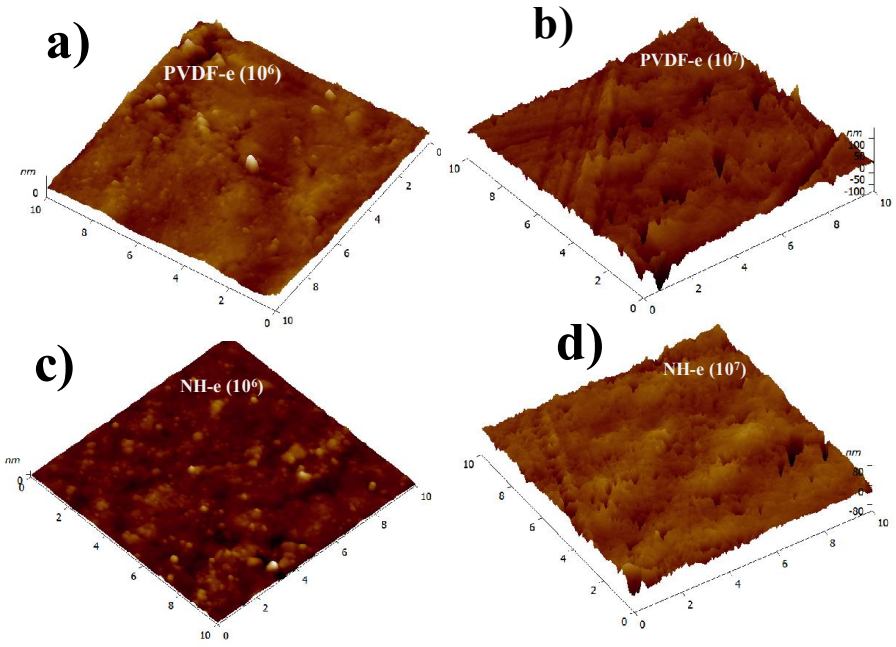

Figure 6.2: Represent the 3-D figure of the etched membrane with fluence variation , the PVDF-e (1×10^6) , PVDF-e (1×10^7), NH-e (1×10^6) and PVDF-e (1×10^7) ions /cm^2 are shown in **(a), (b), (c)** and **(d)** , respectively. We are notifying that the channel dimension and no. of nanochannel is higher in case of the PVDF-7 and NH- 7 etched membrane.

Large number of latent tracks is formed under higher fluence which gets merged and forms bigger channel diameter after etching when compared to low fluence exposed membranes. On the other hand, greater stiffness in presence of two dimensional layered silicates restricts the latent track dimension and, thereby, nanochannel size in nanohybrid under similar fluence is relatively lower. Thus, the nanochannel dimension can be regulated either by using varying fluence or by embedding nanoparticles in the polymer matrix. The channel size increases by enhancing the fluence and the nanochannel dimension can also be reduced considerably in presence of nanoparticles, uniformly distributed in the polymer matrix. This is to mention that pure PVDF and its nanohybrid do not exhibit any channel

even after etching. Hence, irradiation of SHI causes these channels after suitable etching the polymer/hybrid films. The cross-sectional SEM image of NH membrane before and after functionalization is shown in **Figure 6.3 (a-d*).*** The cross-sectional SEM images of the NH membrane before and after styrene monomer grafting and found that the grafting of the nanochannel after treatment of the styrene monomer, shown in image **b & d**, low and high magnification show that grafting of the nanochannel.

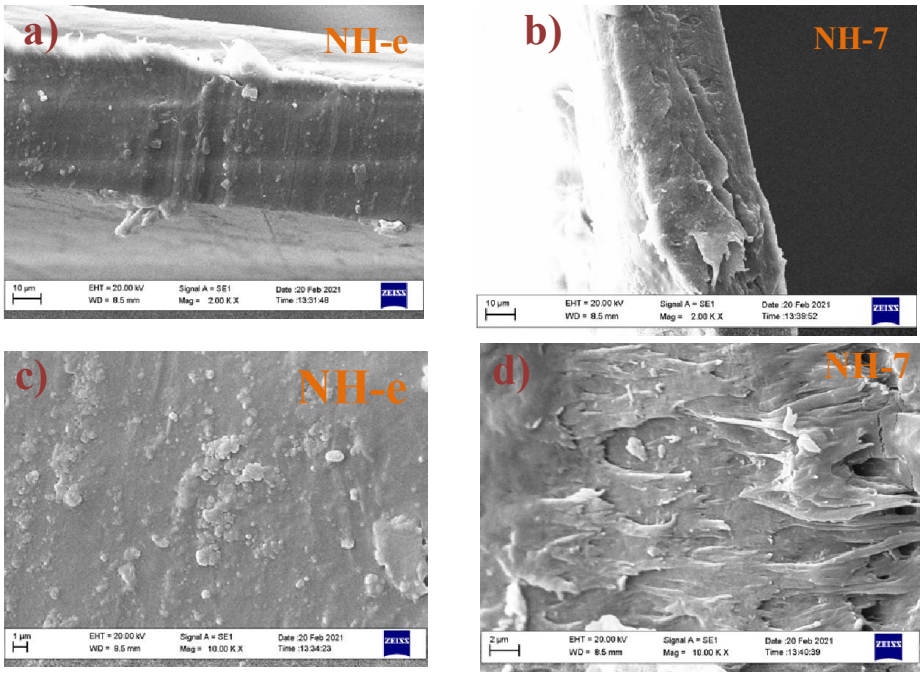

Figure 6.3: Cross-sectional SEM of nanohybrid membrane before and after the styrene grafting followed by the sulphonation. **(a)** Low mag. SEM of NH-e **(b)** low mag.SEM of NH-7 **(c)** High mag. SEM of NH **(d)** High Mag. SEM of NH-7.

6.3.2 Functionalization and evolving of interactive system:

The channels are formed due to irradiation by high energy Li^+ ions of different fluences which expose free radicals at the walls of the channels, after chemical etching of the amorphous tracks. Those free radicals are utilized for grafting of polymer within the nanochannels using vinyl monomer like styrene. Subsequently, the polystyrene chains are functionalized by attaching sulphonate group exclusively within the nanochannels. Three new NMR peaks at chemical shifts of 6.98, 7.04, and 7.18 ppm [1][156] [106] indicate the aromatic proton of polystyrene suggesting grafting of polystyrene on the backbone of PVDF chains probably un-sulphonated styrene polymer but after the sulphonation the ortho - proton of the styrene monomer shifted into the downfield at 7.93 ppm. Beside these peaks the two new peaks at 3.22 ppm and 0.95 ppm are benzylic and aliphatic proton chemical shift respectively. Beside these peaks, four other new peaks are also found at chemical shifts of 1.98, 5.09, 6.29 and 8.13 ppm, presumably due to sulphonate proton in the grafted styrene polymer as shown in **Figure 6.4a** and assigned peak position, along with the characteristics NMR peaks of head-to-head (H-H) and head-to-tail (H-T) of PVDF chain at chemical shift of 2.22 and 2.84 ppm, respectively (**Figure 6.4b**).[98] [213] the extent of sulphonation is calculated using the **equation (1)** and is found to be 10, 15, 10 and 16% for PVDF-6, PVDF-7, NH-6 and NH-7, respectively, indicating greater sulphonation at higher fluence and nanoparticles in hybrid further enhance the degree of sulphonation. NMR spectra of other specimens (PVDF-6, NH-6) are shown in the **Figure 6.4b.**Furthermore ^{13}C and ^{19}F NMR spectra shown in **Figure 6.4c** & **6.4d** of the functionalized membrane against the pristine PVDF support the grafting of the styrene on the polymer chains.[98] In case of the pristine PVDF membrane, the chemical shift at -91.9 ppm and -94.4 ppm

indicate the $CH_2\underline{\mathbf{CF}}_2CH_2$ moiety, are the characteristic peaks of the Head–Tail (H-T) polymerization and chemical shifts at -113ppm,and -117ppm correspond to the $CH_2\underline{\mathbf{CF}_2\mathbf{CF}_2}CH_2$ moiety, arising from the Head–Head (H-H) polymerization and the splitting pattern observed near the Chemical shift of -91.9 ppm due to the decoupling of fluorine with the hydrogen nuclei (supplementary information and references thereof). In functionalized membrane (NH-g-s), few new peaks are observed at -112.3 and 75.1 ppm because of the styrene sulphonated group which shift to higher chemical shift indicating the deshielding effect (downfield shift of the chemical shift) of the fluorine nuclei and at chemical shift at -119 ppm indicates the shielding effect (upfield shift of the chemical shift) of the fluorine nuclei. Due to the presence of styrene proton, the splitting pattern observed near -94.4 ppm marks using the dashed circle the figure below. From the ^{19}F NMR spectra, it is clear that the pristine PVDF membrane functionalized after the SHI-irradiation, chemical etching followed by the styrene grafting and subsequent sulphonation.

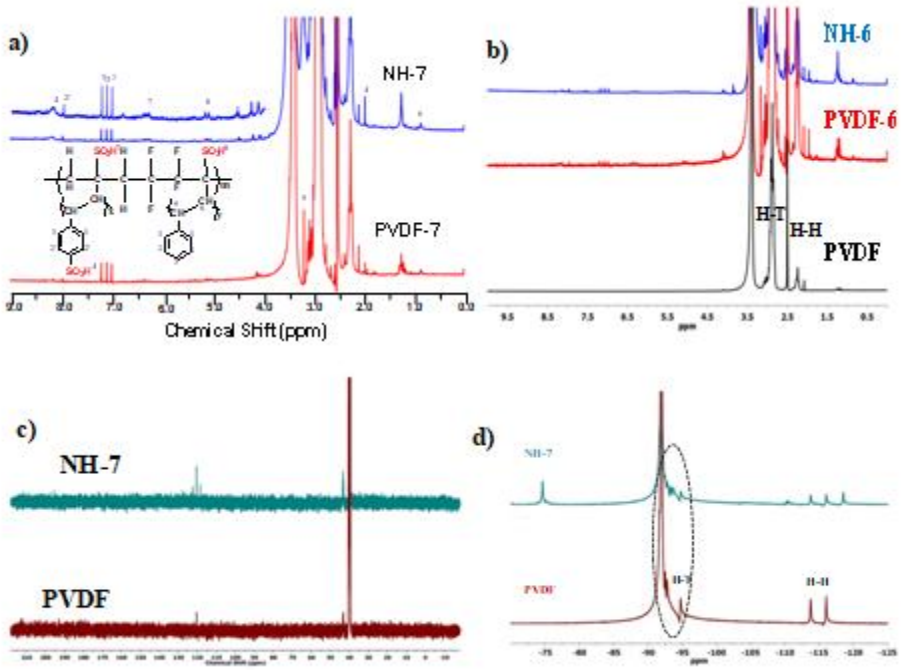

Figure 6.4: The evidence of the grafting (using styrene monomer) followed by their sulphonation confirmed through different NMR nuclei studies, **(a)** the NMR spectra of the PVDF-7, and NH-7 indicating the assignment of possible proton**. (b)**PDVF NMR spectra are given in the ***6.4 (b)*** and PVDF-6 and NH-6***;*** **(c)** ^{13}C-NMR of the functionalized and un-functionalized membrane. In ^{13}C-NMR the three new peaks at chemical shift 118.7, 121.9 and 127.6 ppm indicate the grafting of the styrene monomer on the back bone of the PVDF chain. **(d)** F-19 NMR of the pristine PVDF and its Functionalized (NH-7) membrane.

Figure 6.5a shows FTIR patterns of the samples before and after the grafting and subsequent sulphonation. A typical vibration band at 1642 cm^{-1} confirms the presence of the aromatic ring in grafted specimens along with two more vibration bands at 1045 and 3399 cm^{-1} are due to symmetric vibration of S=O bond of sulphonic acid group both in PVDF-7 / NH-7 and hydrophilic sulphonic group (O–H) present in the functionalized specimens, respectively and similar results also observed in NH-6 and PVDF-6 specimen. It is notable to mention that the vibration bands at 765, 799 and 978 cm^{-1} appear due to α-crystalline phase present in pristine PVDF while metastable electroactive phases (β+γ) have distinctly been presented in nanohybrid and its functionalized samples as observed through their peak position at 838 cm^{-1}.[197][23][218]**Figure 6.5b** represents the *UV–vis* spectra of *PVDF* and *NH* before and after grafting followed by sulphonation. A strong absorption band at 245 nm in *NH* is assigned to $\pi \rightarrow \pi^*$ transition of double bond present in organically modified 2D layered silicate (nanoclay) while there was no absorption peak in pristine *PVDF*. A strong and broad absorption band at 402 and 423 nm in *PVDF-6 and*

PVDF-7, respectively, is due to $n \rightarrow \pi^*$ transition of sulfonate group present in functionalized PVDF. Similar strong red shift along with greater absorption has been observed for *NH-6 and NH-7* specimens at 406 and 555 nm, respectively, mainly due to $n \rightarrow \pi^*$ transition of greater extent of sulfonate groups in nanohybrid vis-à-vis functionalized PVDF.[98]However, *NMR*, *FTIR* and *UV–vis* studies confirm the grafting of polystyrene followed by sulfonation within the nanochannels which eventually conduct electricity and will also be able to capture any metal ion including radionuclides. AFM images of the nanochannels after functionalization appear fully covered up as shown in **Figure 6.5c**. However, the spectroscopic measurements together with surface morphological studies confirm the grafting followed by sulphonation within the nanochannels exclusively making them suitable for possible ion conduction. At this juncture, this is to mention that free radicals are also generated in the surface of the membrane but they are quickly oxidized in presence of ariel oxygen while the free radical within the nanochannels remain active for few hours and the grafting experiment is performed within 1 h after etching.[8]

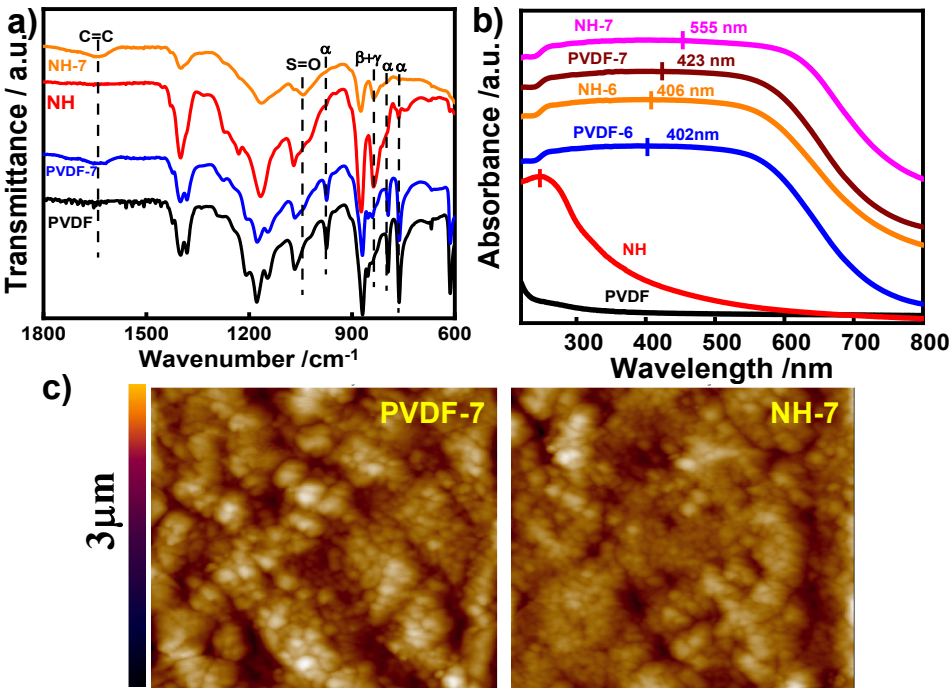

Figure 6.5*:* (a) FTIR spectra of PVDF, NH, PVDF-7, and NH-7 indicating the possible bands for different functionalities and crystalline structure; **(b)** UV spectra of indicated samples, before and after functionalization; and **(c)** Surface morphology through AFM after graft and functionalization shows the coverage of the nanochannels.

6.3.3 Structural modifications and thermal properties:

Chemical modification has been observed within the nanochannel and it is imperative to check whether this modification alter the structure and properties of the membranes. Pristine PVDF crystallizes in common nonpolar α-phase and the peaks at 17.6^0 (020), 18.3^0 (110), and 19.9^0 (111) are consistent with the values reported in the literature (**Figure 6.6a**). In contrast, *PVDF* crystallizes in electroactive β-phase in nanohybrid (NH) in presence of layered silicate (organically modified nanoclay) as evident from the peak position at $2\theta \sim 20.4°$ (200/110).[225][18] The quantification of β–phase is done through the deconvolution of peak and a representative diagram is shown in **Figure 6.6b**. The intensity of the piezoelectric β-phase increases with increase in the degree of grafting and sulphonation both in NH as well as PVDF but the relative enhancement of β–phase in nanohybrid (NH) is significantly higher as compared to PVDF as plotted in **Figure 6.6c**. However, the β-phase fraction is as high as 77% in NH-7 as opposed to meager 24% in PVDF-7 under similar fluence, primarily due to nanoclay induced phenomena and higher functionalization in nanohybrid. The phase conversion into β-phase in nanohybrid arises due to epitaxial crystallization of PVDF chains over the surface of layered silicate, which occurs because of interaction between organically modified layered silicate and polymer

chains, while greater grafting and sulphonation also enhances the β-fraction in nanohybrid. The melting endotherms of PVDF and its nanohybrid before and after functionalization are presented in **Figure 6.6d**. The melting points (T_m) of PVDF and NH decrease after grafting and functionalization due to the formation of β-phase and relatively greater reduction in nanohybrid is presumably due to larger amount of β–phase. This is to mention that β–phase has lower melting temperature than α-phase.[226] Lowering of melting temperature is expected from highly interactive system as well as evident from the lowering of heat of fusion in PVDF (32→28 J/g) and in NH (28 → 19 J/g). The dipoles of sulphonate group and polar PVDF (-CH_2CF_2- linkages) are the origin of the interactive system after grafting and sulphonation. This is worthy to remember that both lowering of melting temperature and reduced heat of fusion arise from a strongly interactive system.[60] [49] So, the greater sulphonation and higher β–phase nucleation in nanohybrid (NH) is responsible for higher reduction of melting as well as heat of fusion. Slightly higher melting temperature of NH (176 °C) as compared to neat *PVDF (174.5 ^oC)* indicates the formation of high melting *γ*-phase induced by nanoclay platelets. Both the heat of fusion and the meting temperature of the nanohybrid membrane explain the thermodynamic mixing of the nanofiller in polymer matrix. Pristine PVDF exhibits spherulitic morphology (**Figure 6.6e**) against needle-like morphology in NH due to the formation of β–phase while significant change in morphology (cloth-like) occurs after irradiation and subsequent functionalization. Thermal stability of PVDF and its nanohybrid membrane before and after functionalization is studied through thermogravimetric analysis (TGA), the normalized weight loss as a function of temperature as shown in **Figure 6.6f**. Pure PVDF degrades at 479 ^oC against 396 ^oC for nanohybrid (NH). On contrary, two step

degradations are observed after functionalization for both PVDF and NH, presumably due to degradation of sulphonate groups (at lower temperature) followed by usual degradation of main PVDF chain at higher temperature.[227] The degradation of sulphonate groups starts at 285, 270, 256 and 226 ^{o}C for PVDF-6, PVDF-7, NH-6, and NH-7, respectively.[22] This early degradation of the sulphonate group in NH-7 membrane indicates the greater extent of sulphonation. However, the membranes are quite stable up to 200 ^{o}C and tiny β-phase makes them suitable for membrane applications.

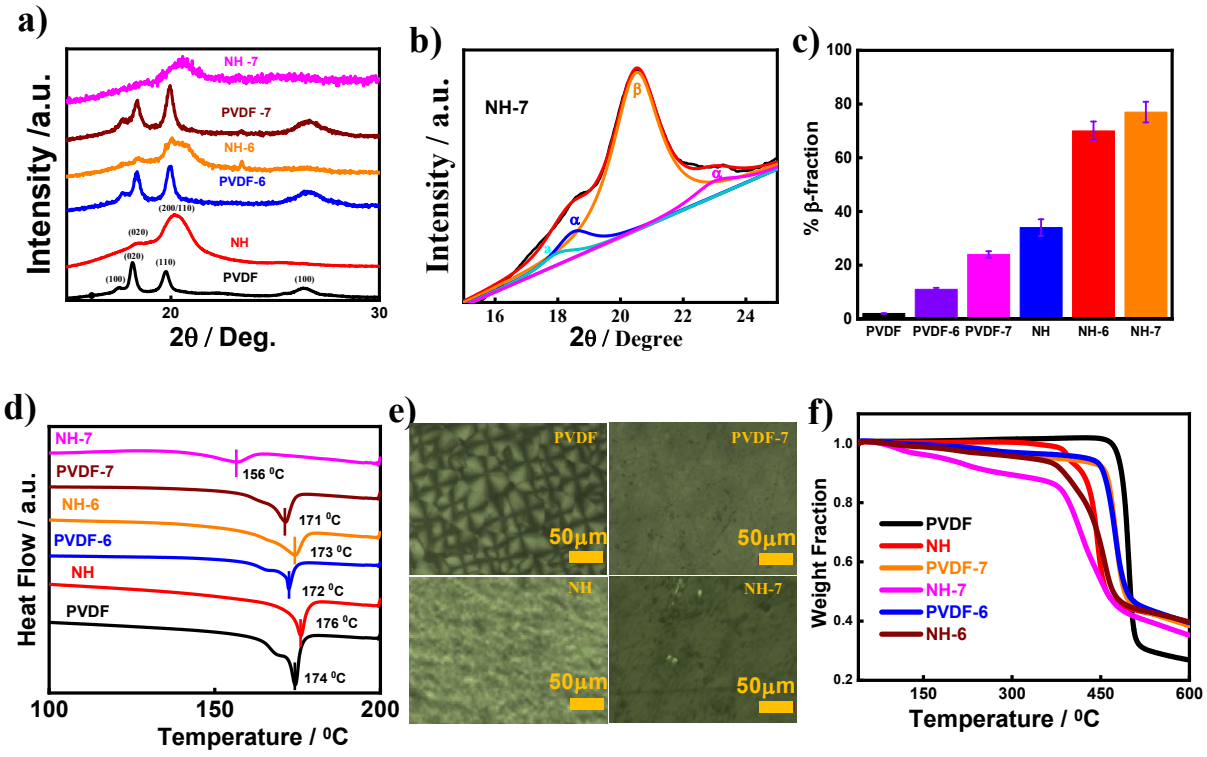

Figure 6.6: Characterization of membrane materials and to provide evidence of the formation of the electro active (piezoelectric) β-phase and thermal stability. **(a)** XRD patterns of PVDF, NH, PVDF-6, NH-6, PVDF-7 and NH-7; **(b)** Deconvolution of a representative XRD spectra of NH-7 showing different phase fraction; **(c)** Piezoelectric β-

content of the different membranes, calculated from the respective deconvulated patterns; **(d)** DSC thermograms of PVDF, NH, PVDF-6, NH-6, PVDF-7 and NH-7 showing the respective melting temperatures; **(e)** Polarizing optical microscopic images of PVDF, NH, PVDF-7 and NH-7; and **(f)** TGA thermograms of PVDF, NH, PVDF-6, NH-6, PVDF-7 and NH-7, indicate their respective degradation temperatures.

6.3.4 Membrane characteristics and electrochemical analysis:

For radionuclide capturing and its recovery from the aqueous solution, water uptake, ion exchange capacity and ion transport are the important characteristic properties of the ionic group (mainly anionic) containing membranes for better ion exchange as well as complexing tendency of the membrane. Ideal membrane should have all three properties such as water uptake, high ion exchange capacity and ions transport efficiency, especially for better radionuclide recovery as well as fuel cell membrane technology. The water uptake of the membranes are found to be 4.9, 5.7, 8.7 and 15 % for PVDF-6, PVDF-7, NH-6, and NH-7, respectively, as shown in the bar diagram **Figure 6.7a** indicating higher water uptake of functionalized nanohybrid as explained from their greater hydrophilic character arising from higher sulphonation. Ion exchange capacities of the membranes are found to be 0.09, 0.09, 0.13 and 0.16 mmole/gram for PVDF-6, PVDF-7, NH-6, and NH-7, respectively, due to greater amount of sulphonated species in the nanohybrid as compared to PVDF membranes (**Figure 6.7b**). Higher values of exchange capacity of nanohybrid membranes clearly suggest their superior radionuclide absorption. Ion fluence has significant effect to enhance the ion exchange capacity. Moreover, EIS (electrochemical impedance spectroscopy) study is used to calculate the proton transport of the ions for different membranes applying the Nyquist plot and is to determine the conductivity of the

membrane using the equation 4 (**Figure 6.7c**). The proton conductivity of the membranes are found to be 0.15 $\times 10^{-2}$, 0.17×10^{-2}, 0.19×10^{-2} and 0.30×10^{-2} S.cm^{-1} for PVDF-6, PVDF-7, NH-6 and NH-7, respectively, at 30 ^{o}C. Generally, ion conduction through the ionic membrane follows two major mechanisms; one of them is due to diffusion of ions from one side to the other side of the membrane, so called, vehicle mechanism, where proton is combined with water molecules present in electrolytes and then diffuses through the membrane and the second mechanism is Grotthuss mechanism where proton transport occurs through hopping. Higher proton conductivity of NH-7 membrane is believed to be due to larger number of sulphonate groups present in the nanochannel which results in significantly higher proton conduction through hopping or diffusion process as compared to PVDF-6 / PVDF-7 membrane for proton conduction. Bode plot (modulus and phase angle as a function of frequency) shows the systematic change of modulus and phase angle with frequency (**Figure 6.7d**). Systematic increase of proton conductivity is observed with increasing temperature maintaining their relative order of conductivity for PVDF and its nanohybrid having higher values for samples irradiated with higher fluence (***Figure 6.7e***). The slope of Arrhenius plot (**Figure 6.7f**) measures the activation energy (E_a) of the specimens and the values are 18.1, 17.9, 11.2 and 11.0 kJ mol^{-1} for PVDF-6, PVDF-7, NH-6, and NH-7, respectively. The summary of membrane characteristics is presented in **Table 6.1.**

Table 6.1: The membrane characteristics such as, ion exchange capacity (IEC), water uptake (WU), and activation energy (Ea) and proton conductivity (km) of the functionalized membranes.

Membrane	IEC (mmole/gram)	WU (%)	Ea(kJ mol^{-1})	k^m (10^{-2} $S.cm^{-1}$)
PVDF-6	0.09	4.9	18.1	0.15
NH-6	0.13	8.7	11.2	0.19
PVDF-7	*0.09*	*5.7*	*17.9*	*0.17*
NH-7	*0.16*	*15.0*	*11.0*	*0.30*

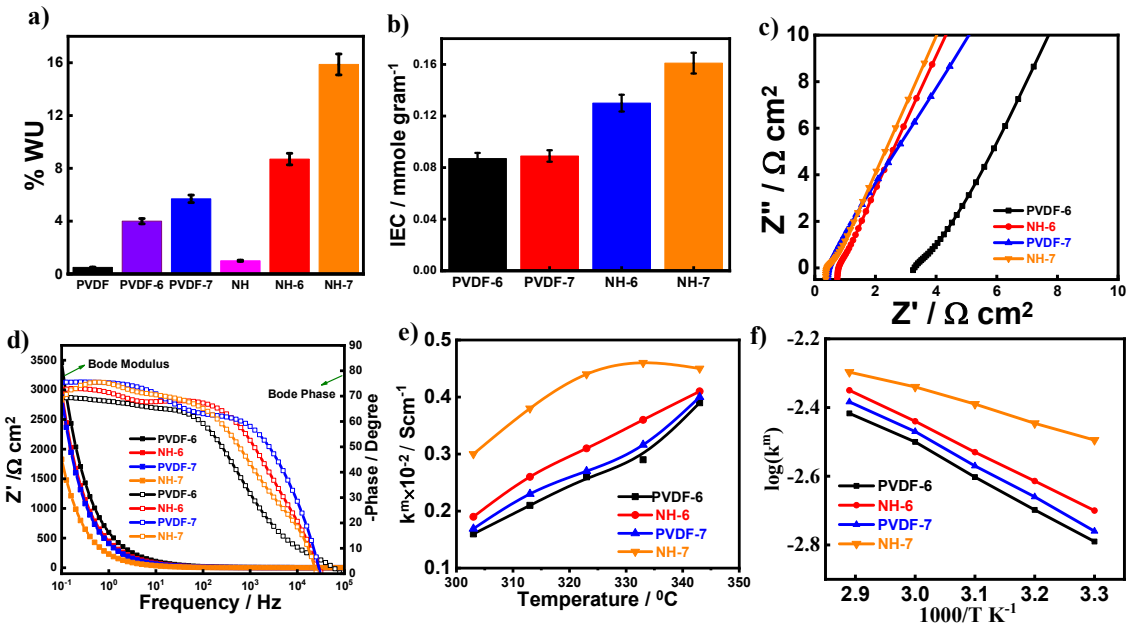

Figure 6.7: Characteristic parameters of the hydrophilic membranes as developed **(a)** Water uptake of the indicated membranes; **(b)**Ion exchange capacity, mmoles/g of the functionalized membranes estimate using the radioactive nuclide CsCl; **(c)** Nyquist Plot of

indicated membranes; **(d)** Bode phase and Bode modulus as a function of frequency of indicated functionalized membranes; **(e)** Proton conductivity variation with temperature of the different membranes as indicated; and **(f)** Arrhenius plot of different membranes for the estimation of activation energy.

The lower value of nanohybrid membranes (11.0 kJ mol−1) by comparison with pristine polymer, point to lowest energy need for the conduction of the proton through the membrane and that ultimately help succeeding easier proton conduction in high fluence functionalized nanohybrid membrane. In std. Nafion the lower activation (10.05 kJ mol^{-1}) energy help the proton transportation through the membrane, high temperature stability becomes an issue for this membrane [1]. Hence, the functionalized nanohybrid membranes are effective for proton conduction as well as good for high temperature applications.

6.3.5 Radionuclide uptake

In this section, studies on radionuclide ($^{241}Am^{3+}$) uptake, surface and depth profiling of ion exchanged (IE) groups in the nanochannels are discussed. Uptake studies for Li^{+} irradiated membranes exhibit ~98% uptake in nearly 1 h with marginal increment noticed in nanohybrid and at higher fluence, as shown in **Figure 6.8a**. Functionalized membranes (both PVDF and NH) show very high uptake values against meager values from the pristine PVDF or NH (**Figure 6.8b**). This is to mention that uptake efficiency is calculated from the concentration of radionuclides present in solution which is converted to 0.584 μg / cm^2 in terms of weight per unit surface area, equivalent to 41.1 mg / g of NH-7 membrane. In this juncture, it is important to understand the effect of nanochannel dimension and uptake efficiency. Less than 80% uptake efficiency, corresponding to 0.35 μg / cm^2, is observed for Ag^{+} (considerably larger size than Li ion) irradiated membrane in a similar

manner. Higher uptake efficiency of Li ion induced membrane is explained from its smaller channel dimension of ~45 nm as opposed to the value of ~60 nm in case of Ag^{+} irradiated membranes. [1] Track densities obtained from alpha radiography for Li^{+} irradiated membrane, as shown in Figure 6.8c, are similar with Ag^{+} irradiated membranes while the track diameter is significantly lower in Li^{+} irradiated membrane (1.6 ± 0.1 μm) vis-à-vis Ag^{+} irradiated membrane (8.0 ± 0.2 μm). However, the number densities of track increase considerably at higher fluence both for PVDF and NH while track dimension decrease in nanohybrid membrane as compared to PVDF (**Figure 6.8c**). Since the number of ion exchange sites are much higher compared to the concentration of $^{241}Am^{3+}$ in solution, this difference cannot be attributed to any possible difference in uptake kinetics and saturation uptake value, even though the track densities and sizes are different.

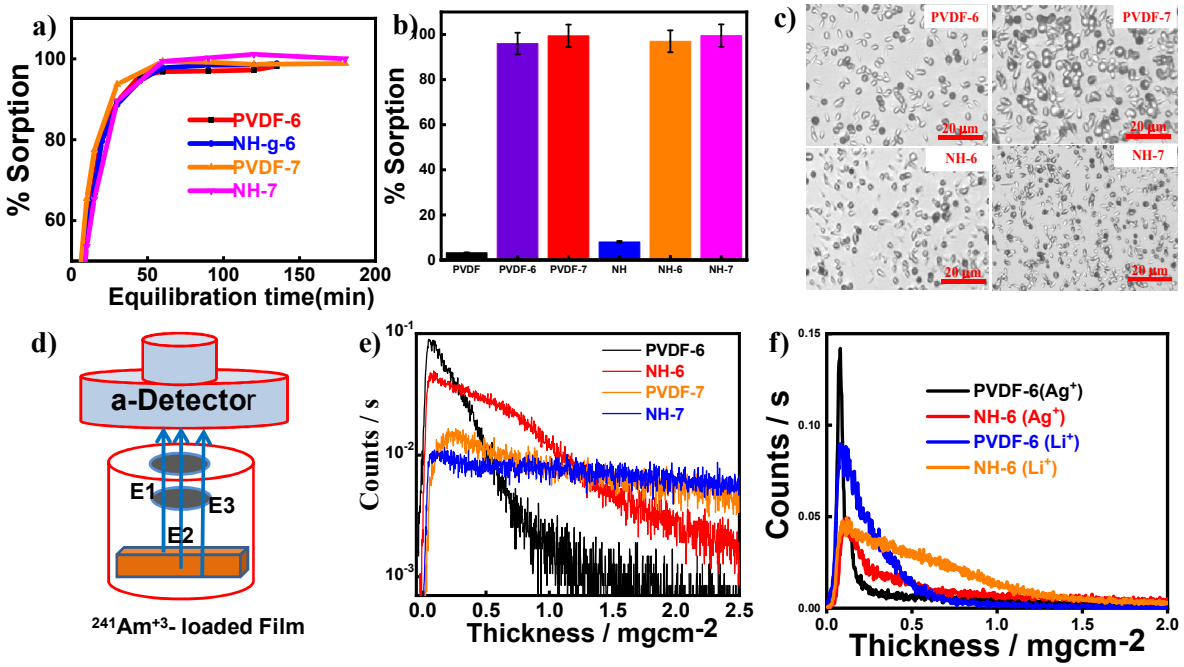

Figure 6.8: Fundamentals of radioactive waste management and the morphology of the functionalized membranes **(a)** Kinetics of sorption of the radioactive Am^{+3} ions using the indicated membranes; **(b)** Uptake of the radioactive Am^{+3} ions comparing with pristine PVDF/NH;**(c)** Radiography of the indicated membranes on the C-39 detector after the uptake measurements; **(d)** Schematic of the alpha spectrometry measurement and energy loss from the different regions; **(e)** the depth profiles of ion exchangeable groups present in the nanochannels for Li^{+} membranes showing fluence dependency in PVDF and its nanohybrid; and **(f)** Comparison of Ag^{+} and Li^{+} ion induced membranes showing the relative depth profile of PVDF and NH irradiated with 1×10^{6} fluence.

6.3.6 Depth profiling of radionuclide within nanochannels:

In order to investigate further the difference in uptake behavior of Li^{+} and Ag^{+} irradiated PVDF/NH membranes, distribution of the ion exchange (IE) groups across the depth of the nanochannels is measured using alpha spectrometry. The energy of alpha particles coming out of the membrane depends on the depth at which the emitting radionuclide is present. Larger is the depth; greater is the energy loss of the alpha particles in the membrane. An arrangement of the alpha spectrometry set-up is shown in ***Figure* 6.8d**. The alpha particles emitted from the film are collimated before entering the detector to minimize the variation of the distance travelled by the alpha particles originating from the same depth but at different angles. The energy loss of the alpha particles in the film is converted into the depth scale using the stopping power or energy loss per unit distance travelled by the alpha particles in the PVDF films, which is calculated using the code SRIM. [228] An average of the stopping power values corresponding to initial alpha particle energy (5.486 MeV) and the energy of the detected alpha particle are used to convert the detected alpha particle

energy in the corresponding depth scale. As thickness of the films is more than the range of the alpha particles in the film, depth profiles are obtained by exposing both surfaces of the film to alpha detector. It should be mentioned here that Alpha Spectrometry obtained from both the surfaces are similar which confirm the through nanochannel formation after the heavy ions irradiation followed by chemical etching (**Figure 6.9 a-c**). The depth profiles of IE groups present in the nanochannel for Li^+ irradiated films are shown in **Figure 6.8e**. With the increasing depth, the energy straggles as well as varies in longer path length in the film resulting in an increasing smearing of the depth profile. The reduction in energy becomes particularly severe as depth approaches the range of alpha particles. Therefore, the depth profiles shown here are limited to 2.5 mg/cm^2 which correspond to 50% of the range of alpha particles in the film. This thickness is also greater than at least 15% of the overall thickness of the film in all the cases and, therefore, can be treated as bulk distribution. It is evident that the depth profile of the IE groups present in the nanochannels depends on fluence and nanoclay in nanohybrid also influences the behavior. Majority of the IE groups are still present close to surface with increasing fluence, even though the bulk functionalization slightly increases. At higher fluence of Li^+ ions, both PVDF-7 and NH-7 show a uniform distribution, with NH-7 being the best in terms of uniformity of the distribution. It should be mentioned here that, though all the Li^+ irradiated films exhibit an uptake of ~98%, NH-7 film shows almost 100% uptake and express lowest smearing raising the prominent influence of nanoclay in hybrid system. In this juncture, it is important to understand the efficiency of channel dimension and a comparison has been made using film irradiated with Ag^+ ion where the channel diameter is of ~70 nm against 50 nm observed in Li^+ ion treated film. A rise in the count rate in the case of Ag^+ irradiated

film (PVDF-7) shows the contribution from the alpha particles coming from the depth closer to the opposite surface indicating comparatively lower thickness of the film (**Figure 6.8f**), showing the most pronounced difference arises from the choice of the ion and influence of nanoclay. The smearing effect is restricted in nanohybrid while smaller dimension of nanochannel in Li^+ membrane continue to show the α-emission from larger depth scale. In the case of Ag^+ irradiated films, IE groups are predominantly present at the near-surface, particularly when exposed to lower fluence (10^6 ions/cm^{-2}). In the case of Li^+ irradiated films, though the distribution is non-uniform at lower fluence, it is much less compared to that of Ag^+ irradiated membrane. As in the case of Ag^+ irradiated films, the presence of nanoclay further decrease this non-uniformity with an increase in the bulk functionalization. It appears that, in the case of Ag^+ irradiated films, the predominant surface functionalization results in a saturation of the uptake due to possibly a reverse migration of the $^{241}Am^{3+}$ into the solution from the film. Such a process may be comparatively much slower or hindered in the case of Li^+ irradiated films, as ions are getting transported deeper into the film. The uptake of $^{241}Am^{3+}$ by Li^+ irradiated films suggest them to be a better choice for complete removal of radionuclides as compared to Ag^+ irradiated films which can explain well the greater uptake by the Li^+ irradiated films. On the other hand, the predominant surface functionalization of Ag^+ irradiated films suggests that these films can be a better candidate for sensing of radionuclides through scintillation mechanism.

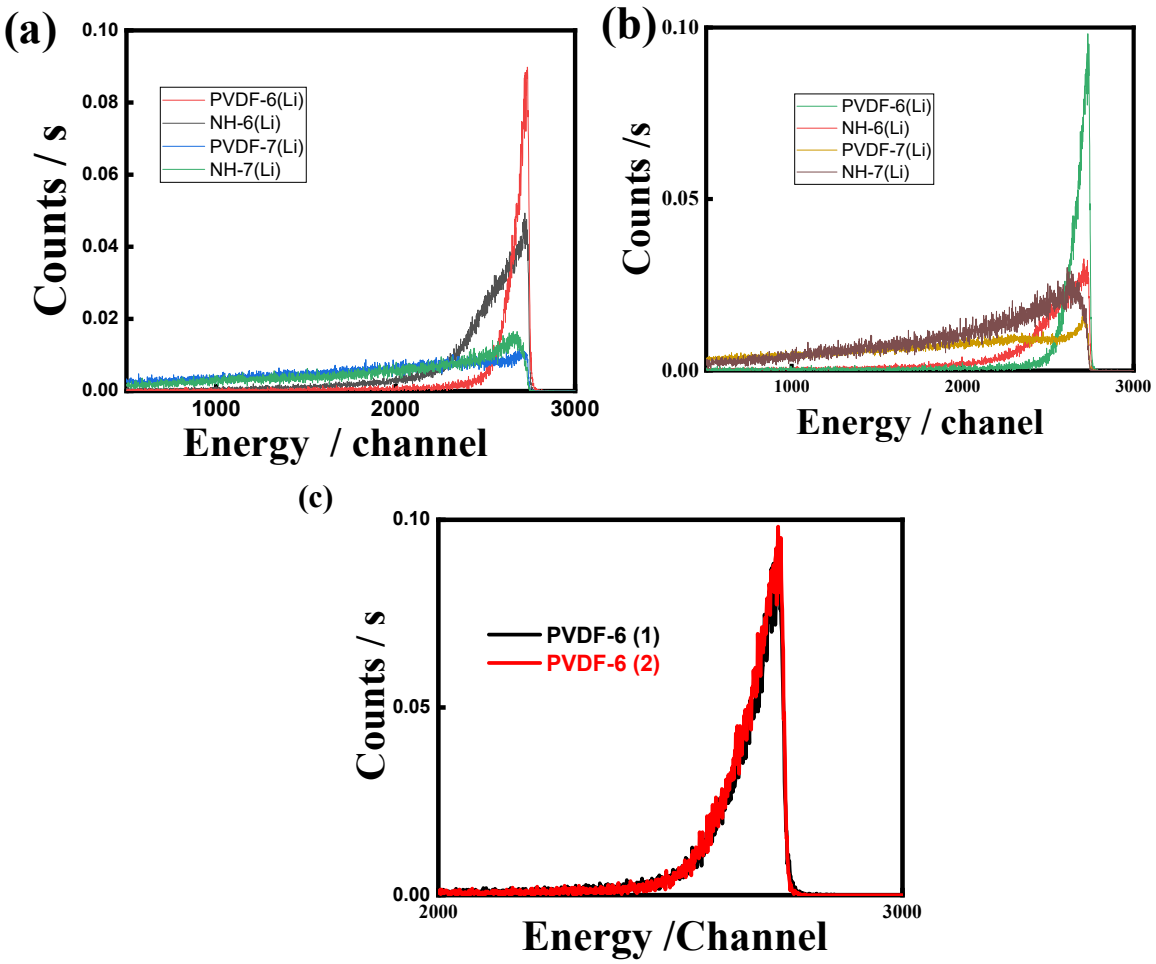

Figure 6.9: Alpha spectrum of the $^{241}Am^{3+}$ Loaded Functionalized membranes **(a)** spectrum recorded side one of membrane; **(b)** spectrum recorded second side of membrane; **(c)** overlap alpha spectrum of the PVDF-6 membrane :the alpha spectrum both side of the Li-ions bombardment, selective chemical etching subsequent grafting of the styrene conducting monomer followed by the sulphonation were recorded and found almost similar pattern of the alpha spectrum, which is conclude that through nanochannel formed. The detail of Fluence, ions and nanoclay variation explanation in manuscripts. In figure **(c)** exact overlap indicate the formation of the through nanochannels.

6.3.7 Sensing of radionuclide using functionalized film:

In order to test the applicability of these films for sensing application, scintillation pulse height spectra are recorded for Ag^{+} and Li^{+} irradiated films with predominant surface functionalization is expected to give best pulse height spectrum. The schematic arrangement for the measurement of pulse height spectrum is shown in **Figure 6.10a**. The $^{241}Am^{3+}$ loaded films is covered with a plastic scintillation film having sufficient thickness to completely stop the alpha particles coming out of the PVDF films. The light photons emitted from the scintillation film are incident at the photo cathode of a photo-multiplier tube (PMT). The pulsed output from the photo-multiplier tube is recorded in a multi-channel analyzer. In order to get an estimate of the detection limit of this film for alpha emitting radionuclides, a comparison of pulse height spectrum along with the background spectrum is shown in **Figure 6.10b**. The detection limit is calculated as $3\sigma_B/CT$, where σ_B is the standard deviation of the background counts above the lower level threshold (marked by the vertical blue line) and CT is the counting time. With a simple set-up and a counting time of 5 min, the detection limit is estimated to be 30 mBq. The pulse height spectra for films irradiated with different fluence of Li^{+} and Ag^{+} ions irradiated membranes are shown in **Figure 6c**. As seen from the figure, for the film irradiated with 10^7 ions/cm^{-2} fluence of Li^{+} has maximum overlap with the noise in the lower channel region. This is expected as most of the alpha particles will be emitted from the bulk of the film (due to the uniform depth distribution) and, therefore, would lose large amount of energy while coming out from the film. This would result in lower scintillation light output from the scintillation film, thereby, reducing the signal pulse height. The situation slightly improves for the film irradiated with lower fluence (10^6 ions/cm^{-2}) of Li^{+}. Compared to the Li^{+} irradiated films,

there is a significant shift of the peak in the pulse height spectra for Ag^{+} irradiated film. The best pulse height spectrum among those, shown in **Figure 6.10c**, is for the film irradiated with 10^{6} fluence of Ag^{+}. This observation is consistent with the maximum non-uniformity of the distribution of $^{241}Am^{3+}$ across the depth of the film with most predominant surface functionalization. Thus, these films can be a very promising candidate for sensing alpha emitting radionuclides and also offer a possibility of remote sensing when coupled with scintillation medium.

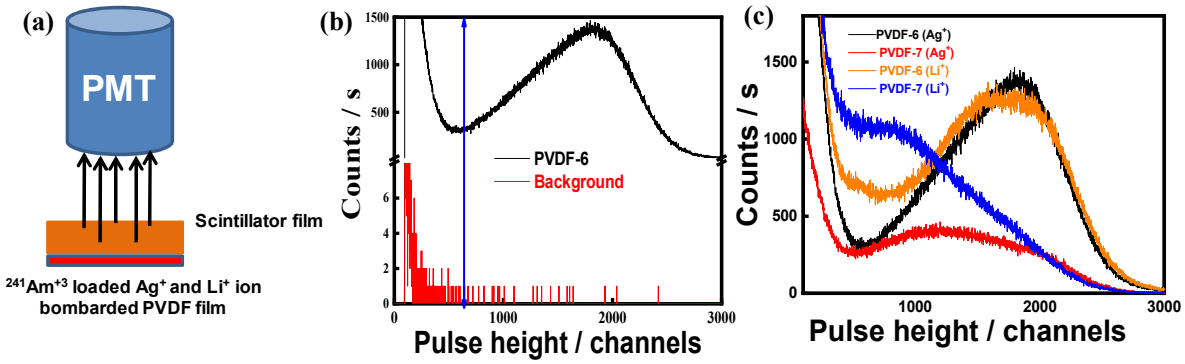

Figure 6.10:(a) The schematic arrangement for the measurement of pulse height spectrum; **(b)** a comparison of pulse height spectrum along with the background spectrum; and **(c)** comparative study of the Ag^{+} and Li^{+} irradiated pulse height spectra of functionalized PVDF-6 PVDF-7 membranes at two different fluence.

6.4 Conclusions:

poly(vinylidene fluoride) and its nanohybrid using two dimensional layered silicate has been prepared through solution route for possible membrane to recover radionuclide from their waste. High energy swift heavy ions from the accelerator have been used to

generate amorphous latent track across the film which is selectively etched by chemical means to create through nanochannels in the film keeping the active free radicals at the periphery of the channel walls. The channel diameter is varied from 40 to 50 nm by changing fluence and by embedding nanoparticles in the polymer matrix. Free radicals are utilized to graft polystyrene within the nanochannels followed by sulphonation in the polystyrene chain to make ion conducting nanochannels suitable to capture radionuclides. The thermal stability and structural details have been worked out including the generation of electroactive β–phase in presence of nanoclay which further increase after functionalization of the membrane. The depression of melting temperature along with reduction of heat of fusion indicate the strongly interactive system as apprised from dipolar interaction between sulphonate group and dipole present in PVDF chains. Electrochemical analyses indicate their high proton conduction and low activation energy of the nanohybrid membrane suitable for better capturing of heavy metals including radionuclides. The proton conductivity of the membrane at 30 ^{o}C is 30 mS.cm^{-1} for nanohybrid which is comparatively higher than pristine as well as the other functionalized membranes. The nanohybrid membrane is expected to be good for the energy application as electroactive phases enhance up to 77%. Functionalized nanohybrid membrane is able to capture nearly ~100% of Am^{3+} from solution and the ion exchange capacity is measured to be 0.16 mmol/gram, comparatively higher than the other functionalized membranes. The distribution of the ion exchange groups in the nanochannels along the depth of the membrane has been measured through alpha spectrometry of the $^{241}Am^{3+}$ loaded films using the energy loss method. These distributions have been compared with those obtained for Ag^{+} irradiated films to understand the difference in uptake behavior and nanochannel

dimension in Li^+ and Ag^+ irradiated films. Nearly uniform distribution of ion exchange groups is observed across the depth of the films irradiated with higher fluence of Li^+ ions. On the other hand, Ag^+ irradiated films show predominant near-surface functionalization, which makes them a promising candidate for sensing alpha emitting radionuclides through scintillation spectroscopy. In the simple set-up and with 5 min counting, a detection limit of about ~30 mBq is achieved for film irradiated with lower fluence of Ag^+ ions.